NeuroImage 127 (2016) 86–96

Contents lists available at ScienceDirect

NeuroImage

journal homepage: www.elsevier.com/locate/ynimg

An integrated framework for targeting functional networks via transcranial magnetic stimulation

Alexander Opitz [a,b,*], Michael D. Fox [c,d,e], R. Cameron Craddock [a,b], Stan Colcombe [a], Michael P. Milham [a,b,*]

[a] Nathan Kline Institute for Psychiatric Research, Orangeburg, NY, USA
[b] Center for the Developing Brain, Child Mind Institute, New York, NY, USA
[c] Berenson-Allen Center for Noninvasive Brain Stimulation, Department of Neurology, Beth Israel Deaconess Medical Center, Harvard Medical School, Boston, MA, USA
[d] Department of Neurology, Massachusetts General Hospital, Harvard Medical School, Boston, MA, USA
[e] Athinoula A. Martinos Center for Biomedical Imaging, Harvard Medical School, Boston, MA, USA

ARTICLE INFO

Article history:
Received 11 August 2015
Accepted 15 November 2015
Available online 19 November 2015

ABSTRACT

Transcranial magnetic stimulation (TMS) is a powerful investigational tool for in vivo manipulation of regional or network activity, with a growing number of potential clinical applications. Unfortunately, the vast majority of targeting strategies remain limited by their reliance on non-realistic brain models and assumptions that anatomo-functional relationships are 1:1. Here, we present an integrated framework that combines anatomically realistic finite element models of the human head with resting functional MRI to predict functional networks targeted via TMS at a given coil location and orientation. Using data from the Human Connectome Project, we provide an example implementation focused on dorsolateral prefrontal cortex (DLPFC). Three distinct DLPFC stimulation zones were identified, differing with respect to the network to be affected (default, frontoparietal) and sensitivity to coil orientation. Network profiles generated for DLPFC targets previously published for treating depression revealed substantial variability across studies, highlighting a potentially critical technical issue.

Introduction

Transcranial magnetic stimulation (TMS) is a noninvasive method for targeted in vivo modulation of neural activity through the induction of electric currents via a rapidly changing magnetic field (Barker et al., 1985). Motivated by the accruing evidence of potential clinical applications in the treatment of psychiatric and neurological disorders (e.g., depression, addiction, Parkinson's disease, stroke), TMS is rapidly emerging in clinical practice. Unfortunately, major technical and methodological questions regarding effective TMS administration remain unaddressed (Fox et al., 2012; Lefaucheur et al., 2014; Opitz et al., 2013; Padberg and George, 2009; Wassermann and Zimmermann, 2012), especially with regard to determine optimal stimulation parameters (number of pulses, strength, etc.). In particular, current approaches to determining which coil location and orientation to use when targeting a given anatomical region or functional system in an individual remain suboptimal.

Efforts to stimulate brain regions with externally observable responses readily demonstrate the importance of both coil location and orientation when attempting to maximize the response to stimulation (Balslev et al., 2007; Brasil-Neto et al., 1992; Opitz et al., 2013; Richter et al., 2013). For example, when stimulating motor cortices, the optimal coil orientation for generation of a motor-evoked potential (MEP) can vary markedly from one individual to the next (Balslev et al., 2007; Opitz et al., 2013; Richter et al., 2013), even if the coil is properly located above a target area (e.g., hand knob). Unfortunately, when attempting to stimulate higher-order multimodal association areas, such as dorsolateral prefrontal cortex (DLPFC), the challenges are two-fold. First, anatomical features and functional localization can be more complex, and second, there are no directly observable physiological responses upon which these two parameters can be optimized. While crude techniques, such as the EEG 10–20 system, are often employed to determine coil location, the usage of anatomical MRI images is an increasing popular approach for improving coil parameter selection (Lancaster et al., 2004; Ruohonen and Karhu, 2010; Sack et al., 2009; Sparing et al., 2008, 2010).

Although helpful, anatomical MRI images alone are not sufficient to guide parameter selection, as the generation of electric currents is impacted by a number of factors not readily apparent from the image. First, brain gyrification creates various transitions between GM and CSF, which differ dramatically in their conductivities; each of these transitions uniquely influences the electric field distribution in an orientation-dependent manner (Thielscher et al., 2011). Second, conductivity anisotropy in large WM fiber bundles leads to preferential directions for current flow, further impacting the electric field generated by TMS and its uniformity (Opitz et al., 2011). These two factors combine to

* Corresponding authors at: Nathan Kline Institute for Psychiatric Research, Orangeburg, NY, USA.
E-mail addresses: aopitz@nki.rfmh.org (A. Opitz), michael.milham@childmind.org (M.P. Milham).

http://dx.doi.org/10.1016/j.neuroimage.2015.11.040
1053-8119/

create a dependency of the electric field distribution on the orientation of the TMS coil. Studies commonly attempt to minimize variability in findings attributable to coil orientation by fixing coil orientation across individuals in a given study. For example, depression studies targeting DLPFC often stimulate at 45 degrees relative to the parasagittal plane—the optimal orientation (on average) for generating motor responses across individuals (Brasil-Neto et al., 1992). Unfortunately, the average ideal orientation for stimulating motor cortex has very little bearing on the ideal orientations for complex higher-order association areas. Additionally, optimization of stimulation parameters based on group averages, rather than the individual, ensures that a non-negligible number of individuals will have suboptimal delivery, which is particularly problematic for clinical applications.

A growing number of realistic computational models of the human head and brain are being developed and employed to optimize TMS targeting on an individual basis. At one extreme is the relatively simplistic spherical model commonly employed in neuronavigation systems, which makes no attempt to account for brain morphometry beyond gross size. At the other extreme is the computationally intensive finite element method (FEM), which can take into account individual brain gyrification and white matter anisotropy—thereby allowing it to account for the impact of coil orientation. While the FEM has been empirically validated (Opitz et al., 2013, 2014), and the coil orientation sensitivities it captures proven to be substantial, the method is yet to be fully adopted by the field. This likely reflects the greater computational expertise and labor required to implement the FEM, combined with the lack of a clear demonstration of their implications for targeting of higher-order association areas.

For higher-order association areas, even if the same anatomical landmarks are consistently targeted across participants, one cannot be sure that the functional roles and associations of the area targeted will be consistent. While there are some relatively well-defined examples of strong anatomo-functional relationships (e.g., stimulation of hand knob impacts hand function), 1:1 relationships are far from the rule in functional neuroanatomy (Goulas et al., 2012; Margulies and Petrides, 2013). Marked regional variation in function among individuals is observed for higher-order, multimodal association networks (e.g., language, cognitive control). A recent innovation to optimize TMS targeting aims to provide a means of assessing the specific functional networks associated with an anatomical location being considered for targeting (Fox et al., 2012, 2014). The approach makes use of resting state fMRI (R-fMRI) approaches to map the functional networks associated with any given location in the brain, thereby allowing researchers to select the ideal anatomical location based upon a priori information about the functional network(s) they would like to target (e.g., subgenual cingulate connectivity). This approach has potential value for efforts to personalize targeting for a given individual (Fox et al., 2013), as well as to compare target selection across research studies and protocols. However, these initial approaches have focused primarily on target location without considering the impact of morphological features and their conductive properties on local electric field strength. As such, precisely targeting networks for stimulation will require a more sophisticated approach.

Here we present an *integrated framework* which combines the finite element modeling approach with resting state fMRI to model the functional systems affected by TMS stimulation at a given coil location and orientation. For the purposes of demonstration, we focus on the dorsolateral prefrontal cortex due to its anatomical complexity and its increasing focus in clinical applications (e.g., depression). We show the utility of this approach in evaluating the network specificity of DLPFC targets employed in the depression literature, and possible dependencies on orientation. We also demonstrate the potential to generate a "stimulation atlas," which can be used to guide researchers and clinicians in decision-making regarding optimal stimulation locations to affect a network of interest on a personalized basis. Additionally, it can provide researchers a tool for generating well-principled hypotheses regarding stimulation, which can be tested using neurophysiological and imaging modalities in human and non-human populations alike.

In order to accomplish our goals and facilitate replication, we make use of 1) high-resolution resting state data from the Human Connectome Project (HCP) (Glasser et al., 2013) to estimate functional connectivity and 2) the openly available SimNibs biophysical modeling package (Windhoff et al., 2013) to estimate the stimulation area of TMS based on the FEM using the high-resolution anatomical and diffusion HCP data on an individualized basis. We demonstrate that targeted resting state networks change in a systematic manner based on coil location and orientation resulting in two largely distinct network stimulation zones. Network profiles of targets employed in the literature vary strongly between studies and may contribute to the variability in treatment outcomes between both studies and patients. Finally, our results can be used as a guideline to target specific network nodes in the DLPFC and concretely inform coil positioning in practice.

Methods

Estimation of TMS stimulation areas

We made use of the high-resolution anatomical MR data from the Human Connectome Project (Glasser et al., 2013; Van Essen et al., 2012) to construct individual FEM models for 25 subjects based on their T1- and T2-weighted images using SimNibs (Windhoff et al., 2013). FEM models distinguish between skin, skull, CSF, GM, and WM and the assigned conductivities were $\sigma_{skin} = 0.465$ S/m, $\sigma_{skull} = 0.010$ S/m, $\sigma_{CSF} = 1.654$ S/m, $\sigma_{GM} = 0.276$ S/m, and $\sigma_{WM} = 0.126$ S/m (Thielscher et al., 2011). For WM, we used anisotropic conductivities derived from the diffusion-weighted images using a volume-normalized approach (Opitz et al., 2011). We simulated a focal Fig. 8 coil (75 mm diameter, C-B60 (Magventure)) as used in Opitz et al. (2013). To cover the full scope of possible stimulated networks and to capture the variability in different DLPFC targeting strategies, we constructed a grid of 25 coil locations centered on BA9 (5 × 5, anterior–posterior and left–right, 1 cm spacing, Fig. 1A) for each subject. For each location, we investigated 12 different coil orientations (15-degree steps) covering a 180-degree half-circle. Due to the symmetry of the electric field to 180-degree coil turns (only the field direction is reversed), it was possible to sample a full 360-degree circle in a computationally efficient manner. For an illustration showing the stimulation grid and investigated coil orientations, see Fig. 1A. For each subject, a total of 300 coil positions (25 placements × 12 orientations) were created and the electric field strength was calculated numerically for each position. An example electric field distribution on the pial surface for one subject is shown in Fig. 1B.

Resting state fMRI preprocessing

Each subject's minimally preprocessed fMRI resting state scan (Glasser et al., 2013) available from the HCP and registered to the MNI space (TR = 0.72 s, 1200 samples, 14.4 min) was further processed using AFNI (Cox, 1996). Processing steps included despiking, slice timing alignment, volume realignment, smoothing with a 4 mm FWHM kernel, motion scrubbing (>0.2 mm per TR), regression of motion parameters, bandpass filtering between 0.01 and 0.1 Hz, and nuisance regression of WM and CSF signals. No global signal regression was performed (Murphy et al., 2009). The resulting residual time series were retransformed to the individual subject space using the available non-linear transformation with FSL FNIRT and were further registered to the pial surface using Freesurfer mri_vol2surf (Fischl et al., 1999).

TMS resting state networks

For each of the 300 coil positions, a seed area was determined based on the corresponding electric field distribution, by selecting those nodes

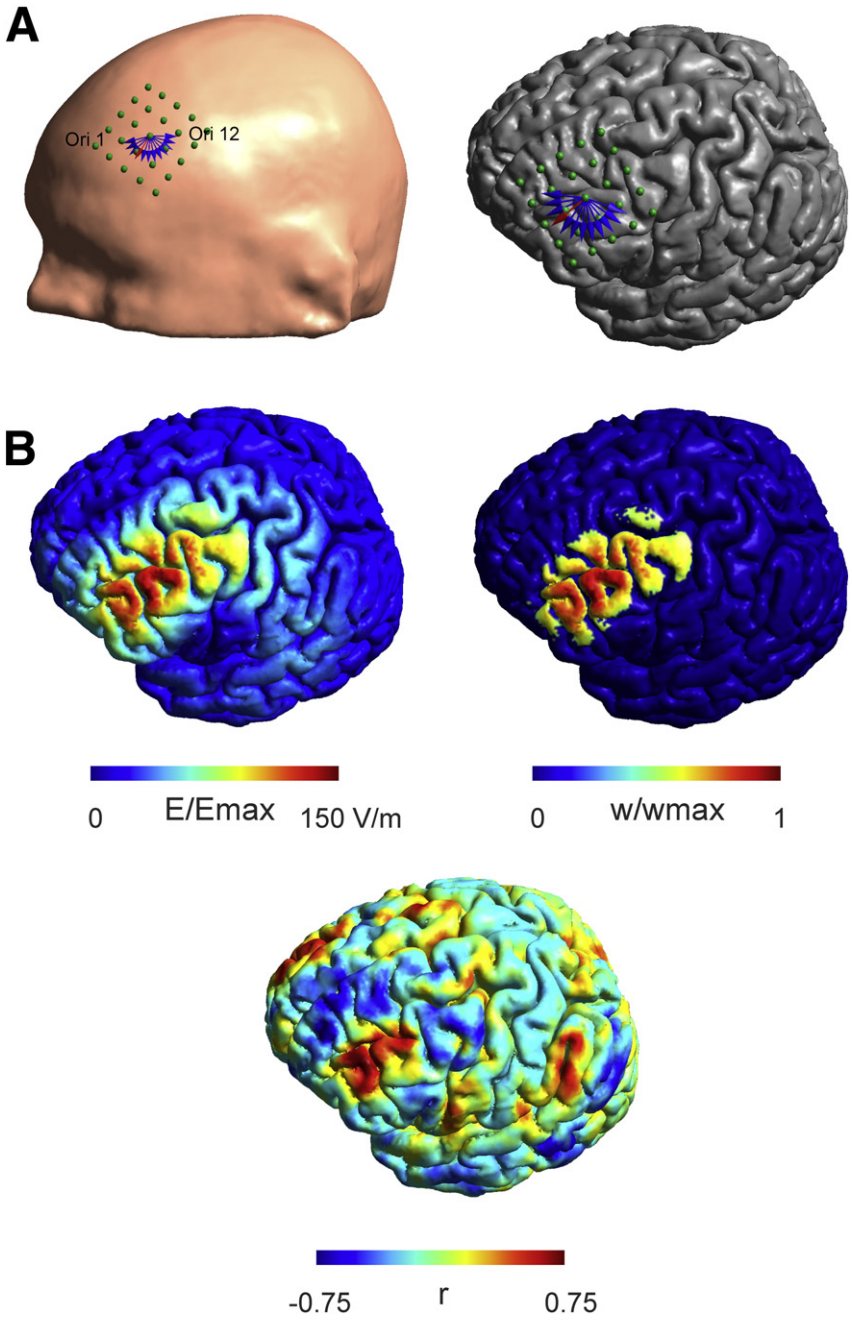

Fig. 1. Stimulation grid placed over the left prefrontal cortex shown for one subject. *A*) 25 points (5 × 5, directions: left–right and anterior–posterior with 1 cm spacing) are aligned along the scalp (left panel). For each location, 12 orientations (15-degree spacing, shown as blue and red arrows displayed at one location. Orientations are numbered counterclockwise from 1 to 12. This convention will be used in later figures) were investigated. The same grid is shown overlaid over the pial surface in the left panel. *B*) Exemplary electric field distribution (left panel) for one coil location and orientation (indicated by the red arrow in Fig. 1A) and associated seed region (right panel). The electric field is typically strongest along the direction of the coil showing a clear orientation dependency. Nodes within the seed region are weighted based on their electric field strength thus taking into account varying degrees of stimulation strength over an extended area. Nodes within the seed region are weighted based on their electric field strength thus taking into account varying degrees of stimulation strength over an extended area. Weights (w) are shown in relation to the maximum weight (wmax). Functional connectivity map for the shown seed region (lower panel). High correlations are visible in frontolateral regions falling inside the seed region but not exclusively limited to it.

that exhibited an electric field strength >50% of the mean over all 300 individual electric field strength maximums on the pial surface. Choosing different electric field thresholds resulted in similar network profiles (Supplementary Fig. 8). In this seed area, a weight was assigned to each node corresponding to the electric field strength at this node divided by the total electric field strength in the seed area. Thus, it was assured that the weights summed to 1 in the seed area for each position. An example for one seed region is shown in Fig. 1B (right panel). For each seed region, a weighted-average time series was computed by summing the time series at each node multiplied by the node's individual weight. The rationale for this method was that it allows us to take into account the spatial extent of the stimulation area as well as the strength of the electric field by giving more weight to those nodes being more strongly stimulated.

We then computed whole-brain functional connectivity maps by correlating the weighted-average time series to the time series of each other node on the pial surface. To enhance the discriminability of different stimulated networks, we used partial correlations with the mean over all 300 averaged time series as a covariate to account for effects of choosing a specific set of coil locations. In addition, we repeated this

step using the standard Pearson correlation to demonstrate that our results are not solely dependent on this specific processing step (Supplementary Fig. 5). An example functional connectivity map is shown in Fig. 1B (lower panel).

An additional analysis was performed using the normal component of the electric field to determine the activation area of TMS (Fox et al., 2004) as seed region. Functional networks were determined in the same manner as for the absolute field strength seed regions. Also, the effect of choosing seed regions derived from spherical FEM models on the predicted networks was investigated (Supplementary Material).

Parcellation of network stimulation zones

To estimate stimulation zones based on the underlying network, we transformed all coil positions into MNI space and their associated network community membership. In a first step, we ignored orientation dependence and averaged network membership over all orientations for each location. In a second step to investigate the influence of coil orientation on network stimulation, we created a parcellation separately for each of the 12 orientations. In addition, to study areas that are highly susceptible to the effects of coil orientations, we calculated for each coil location the standard deviation over all spatial correlations of the 12 functional connectivity maps at each location. Thus, locations whose associated network strongly changes with a differing orientation lead to high values whereas locations that fall into the same network irrespective of coil orientation will lead to low values.

Overlap of TMS networks with established functional networks

As a complementary analysis to our data-driven parcellation of TMS networks, we compared the similarity of our TMS networks with established intrinsic connectivity networks from the literature (Yeo et al., 2011). For that we transformed each of the 300 individual functional connectivity maps for each subject into the average surface space. Then we applied a sparsity threshold of 5% which means that only the strongest 5% of correlation values are kept and binarized the maps. In the following, we computed the dice coefficient between these maps and the seven intrinsic connectivity networks (Yeo et al., 2011) to determine to which extent the TMS networks fall into an established network classification. To enhance the comprehensibility of in total 7500 individual coil positions and associated networks, we clustered them into 9 zones (3×3 grid in MNI space) based on anatomical location. For each zone, we averaged dice coefficients over all locations and in a first step also over all orientations. In a second step, we averaged only over locations but for each orientation separately. To visualize the relative extent to which TMS networks overlap with the ICNs, we used circus (Krzywinski et al., 2009).

Interindividual variability

We next aimed to quantify the interindividual variability in the functional networks involved by TMS that can occur even when coil orientation and location are held constant. In order to accomplish this, we computed the spatial correlation of functional connectivity maps over all subjects using a fixed 45 degrees to midline orientation at the center locations of the 9 zones. This is based on the idea that when interindividual variability is high, the functional connectivity maps of different participants should show low correlation values (strong dissimilarity) and when variability low, they should show high correlation values (high similarity). Correlation values were averaged over all subjects. The same analysis was repeated for the electric field distributions (taking into account only the area where at least one subject exhibited an

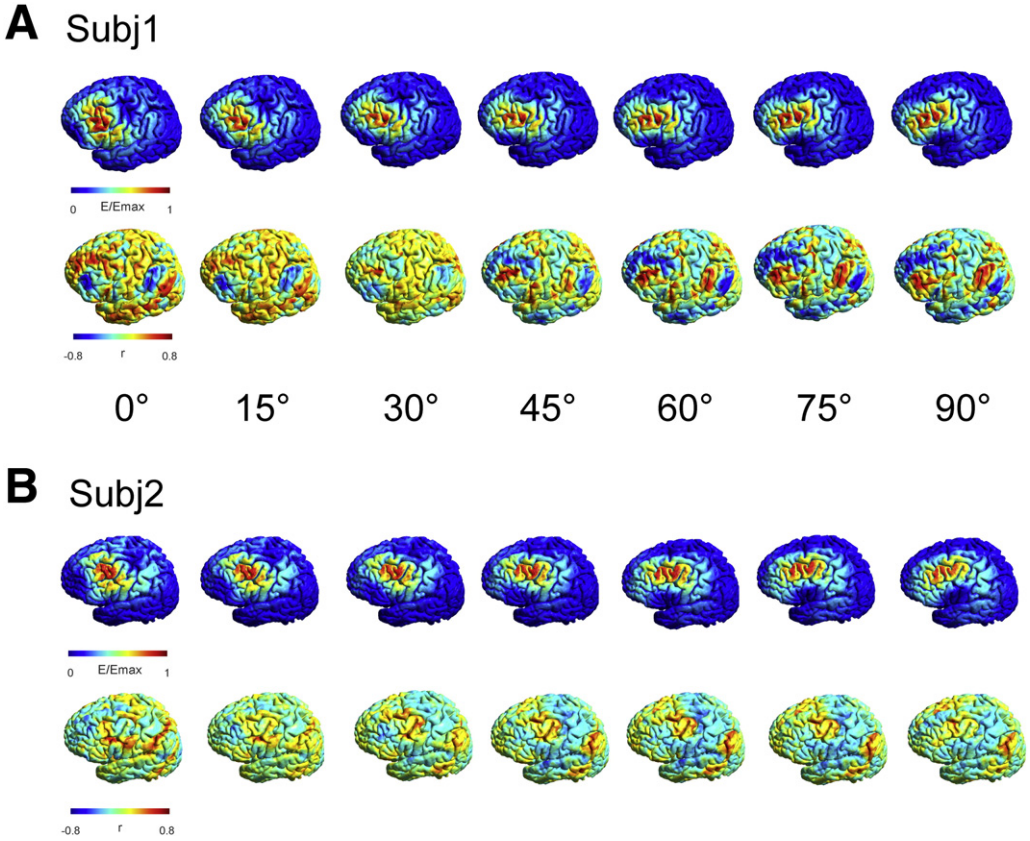

Fig. 2. Exemplary effect of coil orientation on the predicted functional network for two subjects. *A + B*) Electric field distributions for seven different coil orientations (15-degree steps, 90-degree total difference) at the same location (lower panel). While the induced electric field distributions overlap to some extent in the central region common to all orientations, stronger differences occur in the periphery. The functional connectivity maps show a clearly different spatial pattern demonstrating the strong influence of a changing coil orientation on the underlying networks.

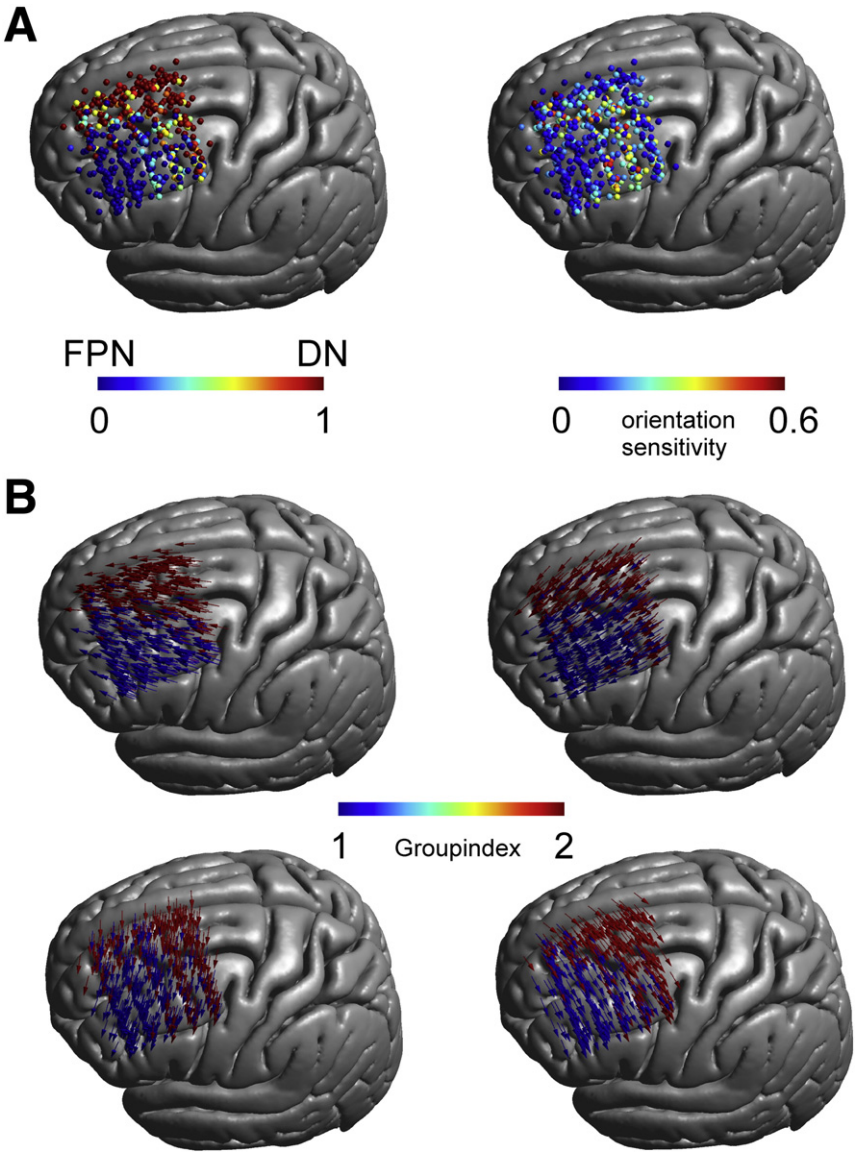

Fig. 3. Network stimulation zones: *A*) Percentage of orientations that fall within the DN compared to the FPN over all subjects and locations (100% FPN relates to 0 [blue], 100% DN relates to 1 [red]). Two stimulation zones are visibly separated by a transition zone in which both networks are partially stimulated (left panel). This transition zone overlaps with a zone of increased orientation sensitivity (right panel) based on the standard deviation of the spatial correlation between functional connectivity maps for differing coil orientations. *B*) Stimulation zones for different coil orientations (shown for 45-degree steps). Depending on coil orientation, the network membership between the FPN and DN changes.

electric field strength > 50% of its maximum) to determine how strongly the electric field distributions vary among individual subjects.

Connectivity profiles of DLPFC Depression targets

In a final analysis, we evaluated the network composition of different targets used in stimulating the DLPFC for treatment of depression. We took the MNI target locations of 11 different targets from Fox et al. (2012), which are based either on group coordinates using anatomical MRIs or anatomical landmarks used in previous studies, and determined the most likely TMS coil location as the closest point on the skin to the MNI target located in the brain. In the following, we averaged for each target position the Dice coefficients for the 7 ICNs of the 20 closest locations (with 12 orientations each). In addition, we evaluated the coil orientation sensitivity of these targets by averaging the coil sensitivity values of the 20 closest coil locations. Increasing the number of locations to 40 or 60 keeps the results unchanged.

Results

Electric field simulations and functional connectivity maps

The electric field predicted by the FEM is strongest on the top of those gyral crowns that are perpendicular to the coil orientation and decreases with increasing sulcal depth (Fig. 1B left panel). As demonstrated in Fig. 2, the predicted electric field showed strong sensitivity to coil orientation which can be detected at the individual participant level for at least a subset of locations. Although the electric field is typically strongest in gyri directly underneath the TMS coil, interactions between anatomy and coil orientation result in substantial deviations from this generalization in many participants—a finding that was previously reported for motor and dorsolateral prefrontal cortices (Opitz et al., 2011, 2013; Thielscher et al., 2011) (see Supplementary Figs. 6–13 for an example of an exception and limitations of spherical symmetric models for detecting these deviations).

In each participant, we used the FEM to generate electric fields for 12 possible orientations at each DLPFC grid location (5 × 5) specified for the individual. For each of the 300 (12 * 25) electric fields maps generated for an individual, we 1) thresholded the map at 50% of the mean maximal electric field strength[1] to identify the area putatively stimulated by the field and 2) used seed-based correlation analysis to determine the R-fMRI-based functional connectivity (iFC) map for the suprathreshold area (see Fig. 1B). The resulting maps were transformed into a common stereotactic space to allow them to be compared between participants. Network community detection performed on these maps identified two key networks that were similar across participants, locations, and orientations: 1) the lateralized frontoparietal network (FPN) commonly observed in task and resting state fMRI studies and 2) the default network (DN) (see supplementary methods).

To quantitatively estimate the impact of coil orientation on the networks stimulated by TMS, we calculated the percentage of orientations at each location that are expected to stimulate the DN, as opposed to the FPN. Our analyses revealed two distinct orientation-invariant zones, one over the lateral–frontal cortex for the FPN and another over the medial prefrontal cortex for the DN (Fig. 3A left panel). Importantly, these two zones were separated by a transition zone, in which the involved network at a given location varied with coil orientation. Fig. 3B illustrates network membership across the locations at select orientations. In order to examine orientation sensitivity beyond network membership, for each participant, we calculated the spatial correlation between the functional connectivity maps associated with the 12 orientations at a given location; the standard deviation of correlations scores was used as a measure of orientation sensitivity. Our findings confirmed the orientation sensitivity of the previously defined transition zone, as well as the orientation insensitivity of the surrounding areas (Fig. 3A right panel).

It is important to underscore that orientation sensitivity was present in a subset of locations for every participant. In order to facilitate an appreciation of orientation variation in the functional network expected to be stimulated at each location on an individual participant basis, we have provided movies for 5 participants (movies can be seen at https://www.youtube.com/channel/UCgEV0odAOV_qIXnfVQgahLA/videos).

Overlap of TMS networks with established networks

A key challenge for TMS targeting is network specificity. Community detection analyses suggested that depending on the specific location within DLPFC, one of two key networks is affected by stimulation. However, significant "collateral stimulation" is likely to occur, with the specifics depending on location and orientation. To address this concern, we reduced the stimulus locations across participants to 9 zones (oriented in a 3 × 3 grid on DLPFC) and created a network connectivity profile for each zone using the 7-intrinsic connectivity network (ICN) parcellation of the brain established by Yeo et al. (2011). Initial analyses only focused on variations related to location, by averaging over all coil orientations (Fig. 4). As indicated by our community detection analyses, the networks expected to be stimulated were dominated by either the FPN (ICN 2) or the DN (ICN 3); specifically, ICN 2 was dominant for the networks expected to be stimulated at lateral DLPFC locations (Z1, Z2, Z4, Z5) while ICN 3 was most prominent for medial and posterior locations. Beyond the FPN and DN, the dorsal attention network (ICN 1) as well as the ventral attention network (ICN 7) was represented in the expected functional connectivity maps depending on location, though to a lesser extent.

Next, we repeated our analyses at each possible orientation. As expected, overlap between the predicted functional connectivity maps

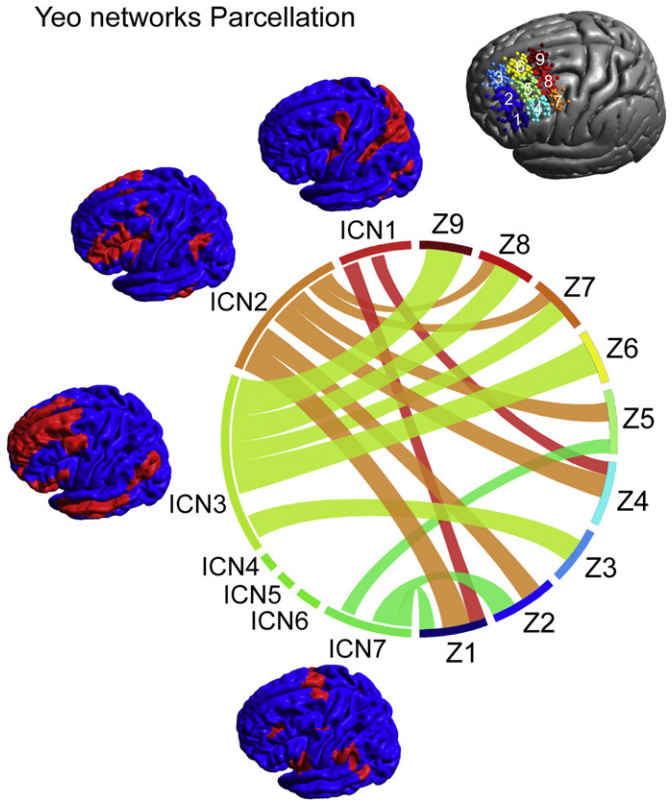

Fig. 4. Overlap of TMS networks with established intrinsic connectivity networks. The relative overlap between the TMS functional connectivity maps with the seven ICNs changes depending on the spatial location. For anterior locations (Z1, Z2, Z4, Z5), the frontal–parietal network (ICN 2) shows the strongest overlap. For medial and posterior regions (Z3, Z6, Z7, Z8, Z9), the default network (ICN 3) shows the strongest overlap with TMS networks. Dorsal (ICN 1) and ventral (ICN 7) attention networks show moderate overlap in frontal locations while other networks (ICN 4: limbic network, ICN 5: visual network, ICN 6: somato-motor network) are not being targeted at any of the investigated coil locations.

for TMS and the 4 ICNs (ICN 1, ICN 2, ICN 3, ICN 7) varied across both orientations and positions (see Fig. 5). For example, the FPN (ICN 2) was preferentially associated with posterior–anterior coil positions, whereas the default network (ICN 3) showed preferential associations with a 45 degrees to midline orientation.

One question that may arise is whether increasing the intensity and thus size of the stimulation area may engage additional networks. In this regard, we found that lowering the stimulation threshold by a factor of 2, which is analogous to doubling the stimulation intensity, did in fact lead to greater inclusion of the remaining 3 networks, particularly somato-motor network (ICN 6). In addition, the ratio between different networks was more uniform, indicating an engagement of a broader range of networks for larger intensities (Supplementary Fig. 8).

Although we only present the group-level analysis results here, it is important to note that these same approaches can be used to create "stimulation atlases" for individual participants. See Supplementary Fig. 4 for two examples.

Connectivity profile of depression targets

We took advantage of a recent review of TMS stimulation sites for the treatment of depression to explore the networks putatively affected by stimulating these regions (Fox et al., 2012). Although each of the 11 stimulation sites evaluated was chosen to target the DLPFC, the network profile of the electric field induced by stimulation at these sites varies substantially and many of these sites fall into orientation-sensitive zones (see Fig. 6). A general trend is visible with the functional connectivity maps for more posterior sites (T1–T4) predominantly falling

[1] We selected 50% as the stimulation threshold based on convention in the modeling literature (e.g. Miranda et al., 2013; Thielscher et al., 2011). Supplementary Fig. 8 demonstrates the general robustness of our findings to threshold selection.

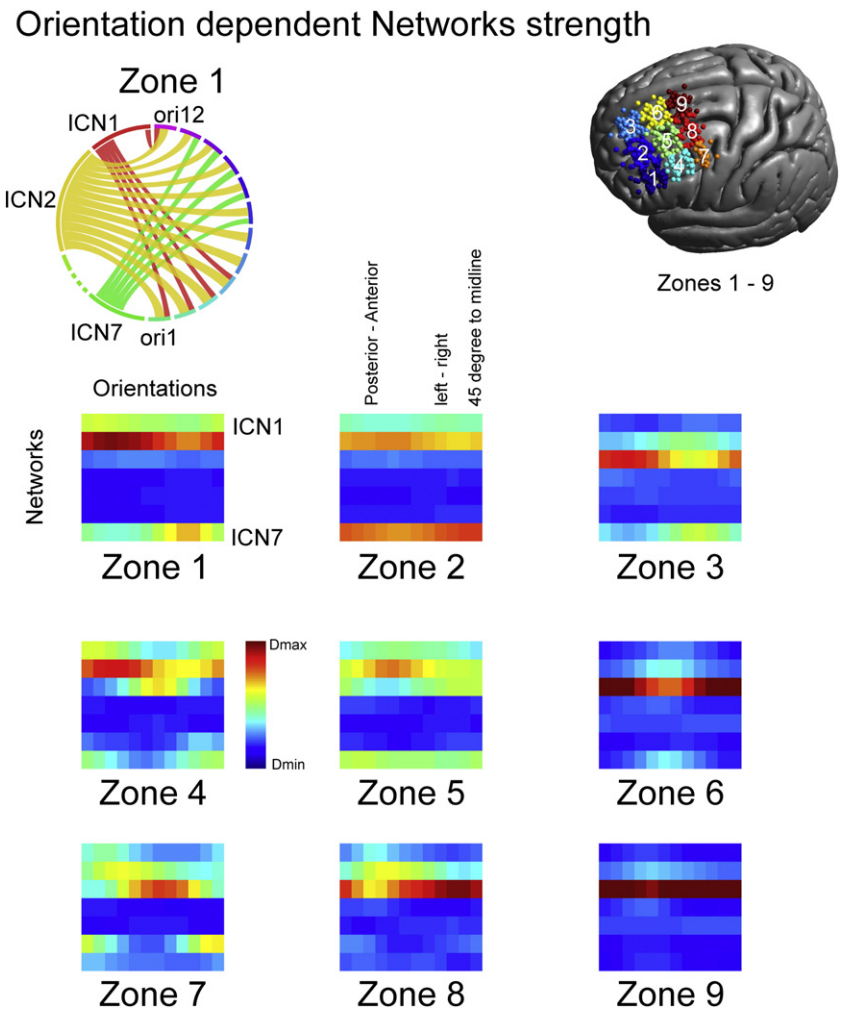

Fig. 5. Coil orientation dependency of intrinsic connectivity networks. Depending on coil orientation (ori), the overlap between TMS and the seven intrinsic connectivity networks changes (strength of dice coefficients color coded with red maximum overlap (Dmax) and blue lowest overlap (Dmin), lower panel). An example demonstrating the coil orientation dependence for Zone 1 is shown on the upper left panel. A network dominance is visible for ICN 2 (FPN) with stronger connections for anterior–posterior connections (orientations 2–5). ICNs 1 and 7 show also some degree of involvement dependent on coil orientation. In general, for the frontal–parietal network, a posterior–anterior coil orientation shows stronger overlap (see e.g. Z1 and Z4), the default network shows stronger overlap with a 45-degree to midline orientation (at Z3, Z6, Z9). Note that coil orientations wrap around at the end of the line.

within the default network, while those for more anterior sites showed higher overlap with the frontoparietal network. In addition, variable overlap with the ventral and dorsal attention network is apparent for different stimulation sites. Interestingly, coil orientation sensitivity is dependent on the location of the TMS sites in general, with more posterior targets being more sensitive to changes in coil orientation whereas most anterior targets exhibited very low orientation sensitivity. These findings emphasize the importance of considering individualized models of TMS when defining stimulation targets for treatment and offer a potential explanation for some of the variability seen for TMS outcomes in depression.

Interindividual variability

Many of the aforementioned studies of depression attempted to limit variability in the functional systems stimulated with TMS, by fixing coil location and orientation across individuals. To assess the likely success of such a strategy, we carried out one final analysis to measure interindividual variation in the maps produced when these parameters are held constant. We found marked differences in functional connectivity maps among participants, particularly in the orientation-sensitive transition zone (Fig. 7). Shown is the mean over the spatial correlations between functional connectivity maps (left panel) and electric field maps (right panel) for different participants calculated for fixed positions and orientation (45 degrees to midline). High values relate to similar maps across individuals and thus lower variability. Importantly, the variability in the FEM models observed across participants for a given location and orientation only partially accounted for the variability in the functional network maps predicted ($r = 0.50$, $p = 0.17$); thus, variation in the functional connectivity maps cannot be predicted by variations in the FEM alone. Side-by-side visualization of the FEM maps and functional network maps obtained for each participant at a fixed site in the transition zone and orientation (set to match the depression studies at 45 degrees), made this point obvious (see supplementary Fig. 7). Thus, personalized modeling of the functional networks targeted by TMS is optimal. However, for studies forced to fix parameters across individuals, our results suggest the value of selecting a location in one of the two orientation-insensitive zones.

Discussion

The present work combined finite element modeling and functional connectivity-based targeting to provide an integrated framework for guiding TMS stimulation. Our initial application of this approach differentiated DLPFC into three zones based upon functional network profiles and orientation sensitivity. Specifically, our analyses revealed 1) an orientation-insensitive anterolateral zone, in which the FPN is the stimulated network; 2) an orientation-insensitive posteromedial zone, in

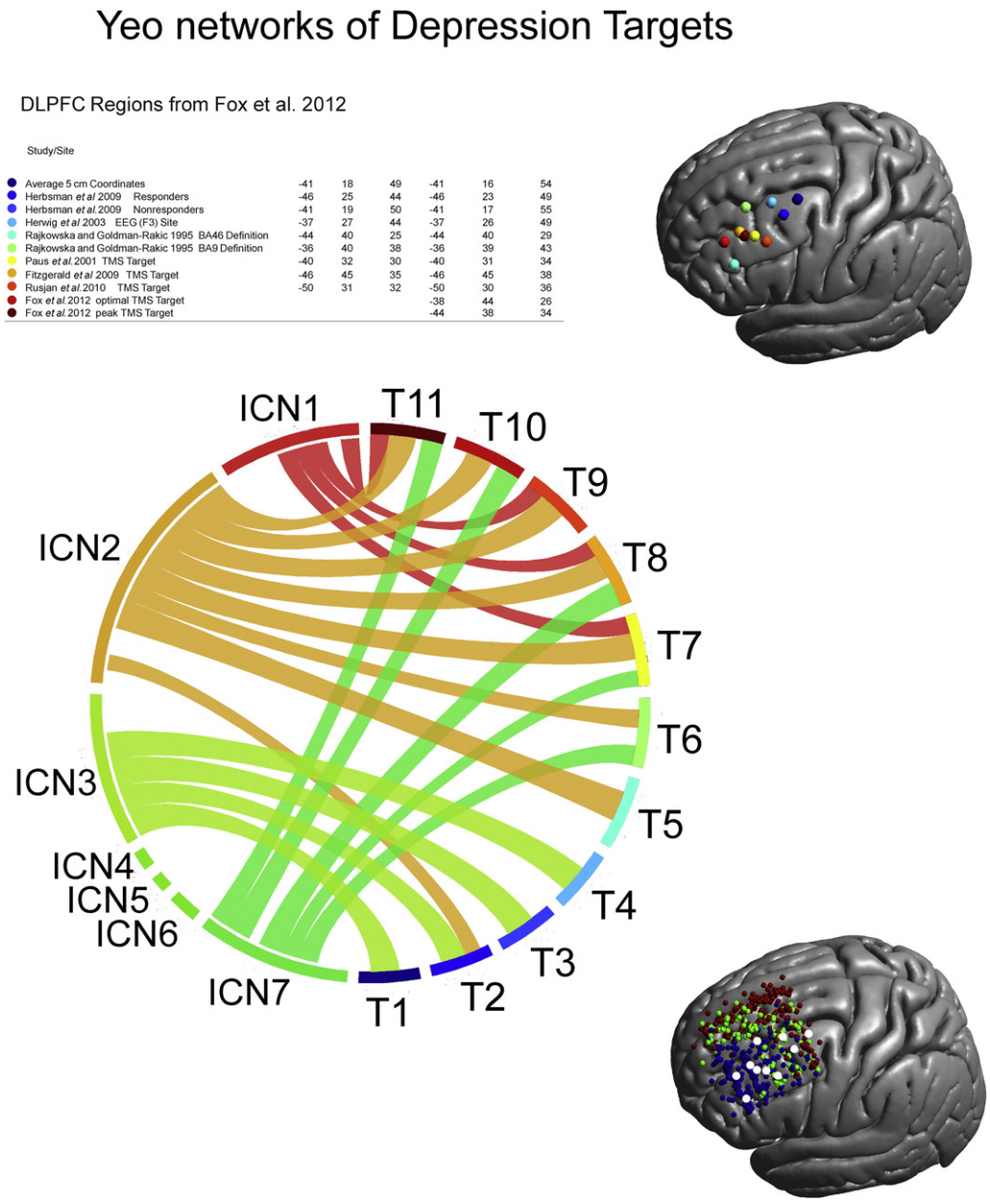

Fig. 6. Network architecture of various depression targets. Employed coil locations (see table and right panel for an illustration) aimed at depression show a high degree of variability. There are roughly two groups of locations falling into either the frontal–parietal or default network. More anterior targets (T7–T11) show also overlap with dorsal and ventral attention networks (ICN1 and ICN7). Depression targets also show a varying degree of coil orientation sensitivity with more posterior targets exhibiting higher sensitivity to coil changes while anterior are largely insensitive to orientation changes (lower right panel, blue region (FPN), red region (DN), green region (orientation-dependent zone)).

which the DN is the stimulated network; and 3) an intermediate zone, in which the relative impact on the DN and FPN varies depending on the coil orientation. Of note is that the coil orientation dependency is only analyzed with respect to the involved functional networks. Effects of differing electric field strength and orientation toward the local neural elements can still cause differences in the effectiveness of stimulation even at orientation independent locations.

The primary analyses in the present work assumed that the absolute electric field strength is the primary determinant of the area of stimulation. However, this assumption is not universally held in the field. In particular, several authors have suggested that the normal component of the electric field (Fox et al., 2004; Janssen et al., 2015; Laakso et al., 2014) is the determinant of the stimulation area, not the field strength. These models differ somewhat in the prediction of stimulation areas, with absolute field strength predicting strongest stimulation at the gyral crowns (Opitz et al., 2011; Thielscher et al., 2011), where the normal component model predicting peak stimulation deeper in the sulci (Fox et al., 2004). Even more complicating, optimal directions differ between MEP generation and plasticity induction at the motor cortex (Sommer et al., 2013). The findings of the present work do not appear to be dependent on which of these factors is modeled, as repetition of our analyses using the normal component of the electric field toward the GM (Fox et al., 2004) instead of field strength yielded highly similar results regarding the networks engaged by TMS, and only some nuanced differences for the coil orientation dependency (see Supplementary Figs. 9–12). Another complicating factor is the effect of the choice of the threshold for which activation of TMS occurs. Future studies could possibly address this issue, which is somewhat complicated as there is

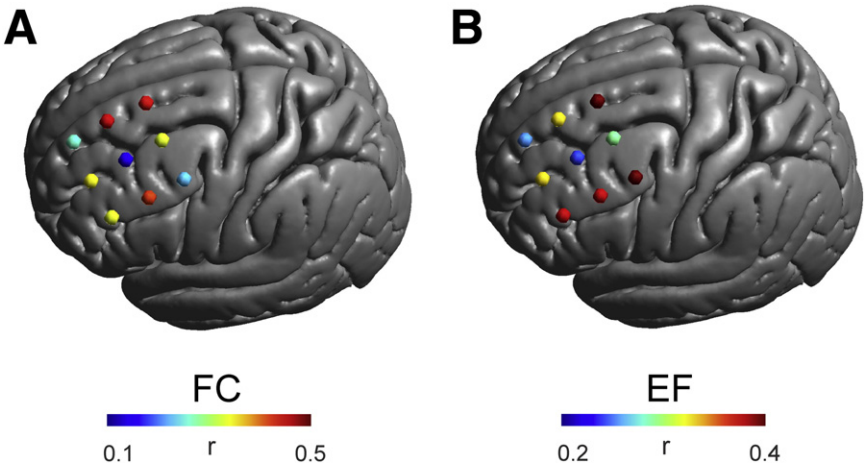

Fig. 7. Interindividual variability in functional networks targeted by TMS. *A*) Mean spatial correlation of functional connectivity (FC) maps over all subjects keeping coil orientation (45 degrees to midline) constant at nine different locations. Interindividual differences vary depending on the brain region with strongest differences lying in a region where several gyri meet (center of the grid). *B*) Variations in the electric field (EF) distribution between subjects. Electric field distributions vary in a similar although not identical manner as functional connectivity maps underscoring the differential variability stemming from both individual anatomy and individual functional architecture.

no clear linear relationship between the absolute electric field strength and outcomes of plasticity inducing protocols(e.g. Doeltgen and Ridding, 2011; Opitz et al., 2015).

It is worth noting that the spherical FEM head model for the electric field calculations (see Supplementary Material) results in network predictions that were similar to those of the realistic models in the areas found to be orientation insensitive. However, there were marked differences in the transition zone, possibly rendering its use in those cases problematic. Additionally, coil orientation sensitivities for the spherical model appeared to be strongly enhanced when compared to the realistic model—especially in the transition zone. This is likely due to the fact that for a spherical FEM model, the electric field direction is only determined by the orientation of the TMS coil; possible interactions of coil orientation and gyrification are not accounted for.

Demonstration of the three network stimulation zones is particularly important when considering the depression literature, where we found that the network profiles calculated for regions stimulated in different studies varied substantially. Of note, for the DLPFC transitional zone, even when coil orientation and location were equated across participants, R-fMRI analyses based on the FEM suggest additional interindividual variation in network profiles. This finding suggests the potential value of integrating functional information in TMS targeting; the next step is for future empirical studies to more definitely prove or disprove this point.

The present work underscores the importance of interindividual variations in anatomy when stimulating higher-order association areas, particularly given that these areas are not associated with any overtly measurable physiological or behavioral response. Theoretical and experimental studies have provided support for the validity and utility of FEM models to account for anatomical variability in stimulation response. Among the most convincing demonstrations of validity are those focusing on the ability of the FEM to explain well-established effects of coil orientation on the generation of motor-evoked potentials (MEPs) at the motor cortex (Opitz et al., 2013; Thielscher et al., 2011) demonstrated the ability of FEM models to explain differential physiological responses toward varying TMS coil orientations in terms of interindividual differences in the curvature of the motor cortex. Perhaps most germane to the present work, Opitz et al. (2014) demonstrated that FEM-predicted TMS stimulation areas overlapped to a high degree with intraoperatively determined motor representations using the gold standard direct electrical stimulation. As suggested in the present work, FEM modeling could be used to ensure that the proper brain region is being stimulated and limit unintended collateral stimulation. Beyond revealing differences in the electric field distributions resulting from anatomical variation, the integrated framework was also able to show that variation of orientation at several locations can actually lead to stimulation of regions with "opposite" (i.e., anticorrelated) connectivity profiles.

The dramatic differences in the network profiles we generated for published TMS targets used in the treatment of depression, with some being primarily weighted toward the DN and others the FPN, merit immediate consideration for future studies and clinical practice. This large variability in the employed targets might explain some of the mixed results in treatment effectiveness observed between studies and subjects. It is worth noting that the coil locations for several studies using the 5 or 6 cm rule, which is used clinically at the present time, fell into the orientation-sensitive zone, where marked variability for the involved networks exists, even when coil orientation and location are held constant. Beyond emphasizing the need for greater consideration of network connectivity profiles in TMS studies, our findings highlight a key gap of knowledge in the existing literature—which network is the more optimal target. Although preliminary studies have begun to relate treatment outcome to stimulation location (Herbsman et al., 2009; Johnson et al., 2013), large-scale, systematic studies of DLPFC targets will be needed before any determination of the optimal network target(s) can be made. Similar approaches have proven successful for deep brain stimulation by relating treatment outcome to anatomical networks (Johansen-Berg et al., 2008; Lujan et al., 2013; Riva-Posse et al., 2014). While in this study we focused on cortical functional networks (in particular, DLPFC), our approach can readily be adapted to subcortical networks as well as already been started in Fox et al. (2012) for the subgenual cingulate. Similarly, functional networks based on task activations could be used for targeting as well, which might lead to similar results due to their similarity to R-fMRI networks (Smith et al., 2009).

Our results suggest the potential for an integrated FEM-imaging framework to serve as a guide to determine TMS coil placement in clinical or research practice. In the absence of FEM and R-fMRI data to personalize coil parameters, our findings suggest that coil placements within regions that have low coil orientation sensitivity may prove fruitful.

Using network-based approaches for targeting TMS has been found successful for enhancement of associative memory based on cortical–hippocampal networks (Wang et al., 2014). Also, the functional connectivity of motor–premotor networks has been found to correlate with MEP latencies for M1 stimulation (Volz et al., 2015) as well as to be predictive for the responsiveness to intermittent theta burst stimulation

(Nettekoven et al., 2015). Thus, taking into account both structural and functional characteristics on an individual subject level to target TMS might prove successful in future studies.

In this study, we have chosen a commonly employed method to derive functional networks using a seed-based approach. Different strategies to derive whole-brain functional networks on an individual level, such as ICA or dual regression, may also be considered in future work. We expect that they will lead to similar results, as all of these approaches are examining the same underlying gross functional architecture based on the temporal correlation of the BOLD signal across different brain regions.

Future experimental work is needed to experimentally test the predictions of our approach. One possibility would be to apply TMS to the DLPFC at different coil locations and orientations in combination with EEG or fMRI and measure whether different functional networks are activated. Alternatively, studies focused on behavioral and clinical outcomes can also be used to test the predictions of the integrated framework. In sum, our integrated targeting approach which takes into account individually unique features of structure and function offers a new rationale to target the DLPFC with TMS that will lead to a more precise application of TMS and possibly more consistent clinical outcomes.

Supplementary data to this article can be found online at http://dx.doi.org/10.1016/j.neuroimage.2015.11.040.

Acknowledgments

This work was supported in part by grants from NIH (U01MH099059) and the Child Mind Institute (1FDN2012-1) to Michael P. Milham, and gifts to the Child Mind Institute (Michael P. Milham) from Phyllis Green, Randolph Cowen, and Joseph P. Healey. Michael D. Fox was supported in part from NIH grants K23 NS083741 and R21 MH099196, and the Sidney Baer Foundation.

Competing interests

A.O. and M.D.F are inventors on patents and patent applications describing methods and devices for noninvasive brain stimulation.

References

Balslev, D., Braet, W., McAllister, C., Miall, R.C., 2007. Inter-individual variability in optimal current direction for transcranial magnetic stimulation of the motor cortex. J. Neurosci. Methods 162, 309–313.

Barker, A.T., Jalinous, R., Freeston, I.L., 1985. Non-invasive magnetic stimulation of human motor cortex. Lancet 1, 1106–1107.

Brasil-Neto, J.P., Cohen, L.G., Panizza, M., Nilsson, J., Roth, B.J., Hallett, M., 1992. Optimal focal transcranial magnetic activation of the human motor cortex: effects of coil orientation, shape of the induced current pulse, and stimulus intensity. J. Clin. Neurophysiol. 9, 132–136.

Cox, R.W., 1996. AFNI: software for analysis and visualization of functional magnetic resonance neuroimages. Comput. Biomed. Res. 29, 162–173.

Doeltgen, S.H., Ridding, M.C., 2011. Low-intensity, short-interval theta burst stimulation modulates excitatory but not inhibitory motor networks. Clin. Neurophysiol. 122, 1411–1416.

Fischl, B., Sereno, M.I., Dale, A.M., 1999. Cortical surface-based analysis. II: inflation, flattening, and a surface-based coordinate system. Neuroimage 9, 195–207.

Fox, P.T., Narayana, S., Tandon, N., Sandoval, H., Fox, S.P., Kochunov, P., Lancaster, J.L., 2004. Column-based model of electric field excitation of cerebral cortex. Hum. Brain Mapp. 22, 1–14.

Fox, M.D., Buckner, R.L., White, M.P., Greicius, M.D., Pascual-Leone, A., 2012. Efficacy of transcranial magnetic stimulation targets for depression is related to intrinsic functional connectivity with the subgenual cingulate. Biol. Psychiatry 72, 595–603.

Fox, M.D., Liu, H., Pascual-Leone, A., 2013. Identification of reproducible individualized targets for treatment of depression with TMS based on intrinsic connectivity. Neuroimage 66, 151–160.

Fox, M.D., Buckner, R.L., Liu, H., Chakravarty, M.M., Lozano, A.M., Pascual-Leone, A., 2014. Resting-state networks link invasive and noninvasive brain stimulation across diverse psychiatric and neurological diseases. Proc. Natl. Acad. Sci. 111, E4367–E4375.

Glasser, M.F., Sotiropoulos, S.N., Wilson, J.A., Coalson, T.S., Fischl, B., Andersson, J.L., Xu, J., Jbabdi, S., Webster, M., Polimeni, J.R., Van Essen, D.C., Jenkinson, M., 2013. The minimal preprocessing pipelines for the Human Connectome Project. Neuroimage 80, 105–124.

Goulas, A., Uylings, H.B.M., Stiers, P., 2012. Unravelling the intrinsic functional organization of the human lateral frontal cortex: a parcellation scheme based on resting state fMRI. J. Neurosci. 32, 10238–10252.

Herbsman, T., Avery, D., Ramsey, D., Holtzheimer, P., Wadjik, C., Hardaway, F., Haynor, D., George, M.S., Nahas, Z., 2009. More lateral and anterior prefrontal coil location is associated with better repetitive transcranial magnetic stimulation antidepressant response. Biol. Psychiatry 66, 509–515.

Janssen, A.M., Oostendorp, T.F., Stegeman, D.F., 2015. The coil orientation dependency of the electric field induced by TMS for M1 and other brain areas. J. Neuroeng. Rehabil. 12, 47.

Johansen-Berg, H., Gutman, D.A., Behrens, T.E., Matthews, P.M., Rushworth, M.F., Katz, E., Lozano, A.M., Mayberg, H.S., 2008. Anatomical connectivity of the subgenual cingulate region targeted with deep brain stimulation for treatment-resistant depression. Cereb. Cortex 18, 1374–1383.

Johnson, K.A., Baig, M., Ramsey, D., Lisanby, S.H., Avery, D., McDonald, W.M., Li, X., Bernhardt, E.R., Haynor, D.R., Holtzheimer III, P.E., Sackeim, H.A., George, M.S., Nahas, Z., 2013. Prefrontal rTMS for treating depression: location and intensity results from the OPT-TMS multi-site clinical trial. Brain Stimul. 6, 108–117.

Krzywinski, M.I., Schein, J.E., Birol, I., Connors, J., Gascoyne, R., Horsman, D., Jones, S.J., Marra, M.A., 2009. Circos: an information aesthetic for comparative genomics. Genome Res. 19, 1639–1645.

Laakso, I., Hirata, A., Ugawa, Y., 2014. Effects of coil orientation on the electric field induced by TMS over the hand motor area. Phys. Med. Biol. 59, 203–218.

Lancaster, J.L., Narayana, S., Wenzel, D., Luckemeyer, J., Roby, J., Fox, P., 2004. Evaluation of an image-guided, robotically positioned transcranial magnetic stimulation system. Hum. Brain Mapp. 22, 329–340.

Lefaucheur, J.P., Andre-Obadia, N., Antal, A., Ayache, S.S., Baeken, C., Benninger, D.H., Cantello, R.M., Cincotta, M., de Carvalho, M., De Ridder, D., Devanne, H., Di Lazzaro, V., Filipovic, S.R., Hummel, F.C., Jaaskelainen, S.K., Kimiskidis, V.K., Koch, G., Langguth, B., Nyffeler, T., Oliviero, A., Padberg, F., Poulet, E., Rossi, S., Rossini, P.M., Rothwell, J.C., Schonfeldt-Lecuona, C., Siebner, H.R., Slotema, C.W., Stagg, C.J., Valls-Sole, J., Ziemann, U., Paulus, W., Garcia-Larrea, L., 2014. Evidence-based guidelines on the therapeutic use of repetitive transcranial magnetic stimulation (rTMS). Clin. Neurophysiol. 125, 2150–2206.

Lujan, J.L., Chaturvedi, A., Choi, K.S., Holtzheimer, P.E., Gross, R.E., Mayberg, H.S., McIntyre, C.C., 2013. Tractography-activation models applied to subcallosal cingulate deep brain stimulation. Brain Stimul. 6, 737–739.

Margulies, D.S., Petrides, M., 2013. Distinct parietal and temporal connectivity profiles of ventrolateral frontal areas involved in language production. J. Neurosci. 33, 16846–16852.

Miranda, P.C., Mekonnen, A., Salvador, R., Ruffini, G., 2013. The electric field in the cortex during transcranial current stimulation. Neuroimage 70, 48–58.

Murphy, K., Birn, R.M., Handwerker, D.A., Jones, T.B., Bandettini, P.A., 2009. The impact of global signal regression on resting state correlations: are anti-correlated networks introduced? Neuroimage 44, 893–905.

Nettekoven, C., Volz, L.J., Leimbach, M., Pool, E.M., Rehme, A.K., Eickhoff, S.B., Fink, G.R., Grefkes, C., 2015. Inter-individual variability in cortical excitability and motor network connectivity following multiple blocks of rTMS. Neuroimage 118, 209–218.

Opitz, A., Windhoff, M., Heidemann, R.M., Turner, R., Thielscher, A., 2011. How the brain tissue shapes the electric field induced by transcranial magnetic stimulation. Neuroimage 58, 849–859.

Opitz, A., Legon, W., Rowlands, A., Bickel, W.K., Paulus, W., Tyler, W.J., 2013. Physiological observations validate finite element models for estimating subject-specific electric field distributions induced by transcranial magnetic stimulation of the human motor cortex. Neuroimage 81, 253–264.

Opitz, A., Zafar, N., Bockermann, V., Rohde, V., Paulus, W., 2014. Validating computationally predicted TMS stimulation areas using direct electrical stimulation in patients with brain tumors near precentral regions. Neuroimage Clin. 4, 500–507.

Opitz, A., Legon, W., Mueller, J., Barbour, A., Paulus, W., Tyler, W.J., 2015. Is sham cTBS real cTBS? The effect on EEG dynamics. Front. Hum. Neurosci. 8.

Padberg, F., George, M.S., 2009. Repetitive transcranial magnetic stimulation of the prefrontal cortex in depression. Exp. Neurol. 219, 2–13.

Richter, L., Neumann, G., Oung, S., Schweikard, A., Trillenberg, P., 2013. Optimal coil orientation for transcranial magnetic stimulation. PLoS One 8, e60358.

Riva-Posse, P., Choi, K.S., Holtzheimer, P.E., McIntyre, C.C., Gross, R.E., Chaturvedi, A., Crowell, A.L., Garlow, S.J., Rajendra, J.K., Mayberg, H.S., 2014. Defining critical white matter pathways mediating successful subcallosal cingulate deep brain stimulation for treatment-resistant depression. Biol. Psychiatry 76, 963–969.

Ruohonen, J., Karhu, J., 2010. Navigated transcranial magnetic stimulation. Neurophysiol. Clin. 40, 7–17.

Sack, A.T., Cohen Kadosh, R., Schuhmann, T., Moerel, M., Walsh, V., Goebel, R., 2009. Optimizing functional accuracy of TMS in cognitive studies: a comparison of methods. J. Cogn. Neurosci. 21, 207–221.

Smith, S.M., Fox, P.T., Miller, K.L., Glahn, D.C., Fox, P.M., Mackay, C.E., Filippini, N., Watkins, K.E., Toro, R., Laird, A.R., Beckmann, C.F., 2009. Correspondence of the brain's functional architecture during activation and rest. Proc. Natl. Acad. Sci. U. S. A. 106, 13040–13045.

Sommer, M., Norden, C., Schmack, L., Rothkegel, H., Lang, N., Paulus, W., 2013. Opposite optimal current flow directions for induction of neuroplasticity and excitation threshold in the human motor cortex. Brain Stimul. 6, 363–370.

Sparing, R., Buelte, D., Meister, I.G., Paus, T., Fink, G.R., 2008. Transcranial magnetic stimulation and the challenge of coil placement: a comparison of conventional and stereotaxic neuronavigational strategies. Hum. Brain Mapp. 29, 82–96.

Sparing, R., Hesse, M.D., Fink, G.R., 2010. Neuronavigation for transcranial magnetic stimulation (TMS): where we are and where we are going. Cortex 46, 118–120.

Thielscher, A., Opitz, A., Windhoff, M., 2011. Impact of the gyral geometry on the electric field induced by transcranial magnetic stimulation. Neuroimage 54, 234–243.

Van Essen, D.C., Ugurbil, K., Auerbach, E., Barch, D., Behrens, T.E., Bucholz, R., Chang, A., Chen, L., Corbetta, M., Curtiss, S.W., Della Penna, S., Feinberg, D., Glasser, M.F., Harel, N., Heath, A.C., Larson-Prior, L., Marcus, D., Michalareas, G., Moeller, S., Oostenveld, R., Petersen, S.E., Prior, F., Schlaggar, B.L., Smith, S.M., Snyder, A.Z., Xu, J., Yacoub, E., 2012. The Human Connectome Project: a data acquisition perspective. Neuroimage 62, 2222–2231.

Volz, L.J., Hamada, M., Rothwell, J.C., Grefkes, C., 2015. What makes the muscle twitch: motor system connectivity and TMS-induced activity. Cereb. Cortex 25, 2346–2353.

Wang, J.X., Rogers, L.M., Gross, E.Z., Ryals, A.J., Dokucu, M.E., Brandstatt, K.L., Hermiller, M.S., Voss, J.L., 2014. Targeted enhancement of cortical-hippocampal brain networks and associative memory. Science 345, 1054–1057.

Wassermann, E.M., Zimmermann, T., 2012. Transcranial magnetic brain stimulation: therapeutic promises and scientific gaps. Pharmacol. Ther. 133, 98–107.

Windhoff, M., Opitz, A., Thielscher, A., 2013. Electric field calculations in brain stimulation based on finite elements: an optimized processing pipeline for the generation and usage of accurate individual head models. Hum. Brain Mapp. 34, 923–935.

Yeo, B.T., Krienen, F.M., Sepulcre, J., Sabuncu, M.R., Lashkari, D., Hollinshead, M., Roffman, J.L., Smoller, J.W., Zollei, L., Polimeni, J.R., Fischl, B., Liu, H., Buckner, R.L., 2011. The organization of the human cerebral cortex estimated by intrinsic functional connectivity. J. Neurophysiol. 106, 1125–1165.